Many-body physics with individually controlled Rydberg atoms

Antoine Browaeys [iD]* and Thierry Lahaye

Recent decades have witnessed great developments in the field of quantum simulation—where synthetic systems are built and studied to gain insight into complicated, many-body real-world problems. Systems of individually controlled neutral atoms, interacting with each other when excited to Rydberg states, have emerged as a promising platform for this task, particularly for the simulation of spin systems. Here, we review the techniques necessary for the manipulation of neutral atoms for the purpose of quantum simulation—such as quantum gas microscopes and arrays of optical tweezers—and explain how the different types of interactions between Rydberg atoms allow a natural mapping onto various quantum spin models. We discuss recent achievements in the study of quantum many-body physics in this platform, and some current research directions beyond that.

Many-body physics studies the behavior of ensembles of interacting quantum particles. This is a broad area encompassing almost all condensed-matter physics, but also nuclear and high-energy physics. Despite the immense successes obtained over recent decades, many phenomena observed experimentally still do not have a fully satisfactory explanation. At the origin of the difficulty to derive macroscopic properties from the microscopic laws governing the interactions between particles lies the exponential scaling of the size of the Hilbert space with their number. In practice, the best known ab initio methods allow the calculation of the evolution of fewer than 50 particles. To investigate relevant questions involving a much larger number of particles (after all, even 1 mg of usual matter already contains 10^{18} atoms!), one must rely on approximations, and the art of solving the many-body problem largely relies on mastering them. However, using approximations is not always possible and it may be hard to assess their range of validity.

One approach to move forward was suggested by Richard Feynman[1] and consists of building a synthetic quantum system in the lab and implementing a model of interest for which no other way to solve it is known. The model may be an approximate description of a real material, but it can also be a purely abstract one. In this case, its implementation leads to the construction of an artificial many-body system, which becomes an object of study on its own. One appealing feature of this approach is the ability to vary the parameters of the model in ranges inaccessible otherwise, thus providing a way to better understand their respective influence. For example, if one is interested in the role of interatomic interactions on the phase of a given system, synthetic systems become interesting as they allow the variation of their strength in a way that is usually impossible in real materials. The approach introduced by Feynman is usually referred to as quantum simulation[2,3], but it can be viewed more generally as exploring many-body physics with synthetic systems: in the same way chemists design new materials exhibiting interesting properties (such as magnetism, superconductivity), physicists assemble artificial systems and study their properties, with the hope of observing new phenomena.

For a long time, this idea remained theoretical as the experimental control over quantum objects was not advanced enough. The situation has changed radically in the past 20 years with the development of experimental techniques that allow the control of the quantum state of individual quantum objects, be they atoms, molecules, ions, photons or even artificial atoms such as quantum dots, superconducting circuits or excitons in semiconductors, to name a few[3]. For all these platforms, physicists designed sets of tools that allow the control of individual 'atoms', as well as the ability to tune their interactions. This led to the idea of programmable quantum simulation where all the parameters of the Hamiltonian one wants to implement are tunable. But these synthetic systems can also be viewed as machines able to prepare quantum states that are useful for many applications. For example, they can generate large entangled states, whose correlations are useful to beat the standard quantum limit, hence leading to clocks or sensors with enhanced precision[4]. In the long-term, they could lead to quantum computers, with each 'atom' carrying a quantum bit[5,6]. Interestingly, machines able to implement spin models could be useful to answer computationally hard problems well beyond physics, such as combinatorial optimization problems—the travelling salesman's problem being one prominent example. Many of these optimization problems can be cast as Ising models[7], which most quantum simulators implement naturally. By varying the parameters in the experiment, one could drive the system into a state encoding the solution of the problem.

Among all the platforms being developed (many of which have been reviewed recently[8–12]), this Review focuses on ensembles of individual atoms trapped in optical lattices or in arrays of microscopic dipole traps separated by a few micrometres. In this platform, the atoms are almost fully controllable by optical addressing techniques. To make them interact at distances larger than a micrometre, they are excited to Rydberg states, that is, states with large principal quantum numbers n (refs. [13,14]). When in this state, they feature two important properties. First, their lifetime, scaling as n^3, is much longer than that of the low-lying transitions (typically in the 100 μs range for $n \approx 50$). Second, they exhibit large dipole moments between states n and $n-1$ with opposite parity, scaling as n^2. This leads to large interaction strengths V, corresponding to frequencies $V/h \gtrsim 1$ MHz (where h is Planck's constant) for $n \approx 50$ at distances around 5 μm. As we will see in this Review, these ensembles of interacting atoms naturally implement spin models, one of the simplest (and probably most thoroughly studied) many-body systems.

Laboratoire Charles Fabry, Institut d'Optique Graduate School, CNRS, Université Paris-Saclay, Palaiseau, France. *e-mail: antoine.browaeys@institutoptique.fr

After introducing the concept of the Rydberg blockade and the techniques used to prepare and manipulate arrays of single atoms, we describe the various types of interactions at play between Rydberg atoms. We then review quantum simulation experiments dealing with the Ising and XY spin models, and conclude by discussing the perspectives opened by the recent developments of the field.

Rydberg blockade

The study of Rydberg atoms played an important role in the early days of atomic physics and in the development of quantum mechanics. A second 'golden age' of Rydberg physics started when tunable lasers became available in the 1970s—the strong coupling of Rydberg atoms to electromagnetic fields made them an ideal testbed for understanding atom–light interactions, culminating in the birth of cavity quantum electrodynamics[15]. At this stage, interactions between Rydberg atoms, although observed as early as 1981 in dense Rydberg gases[16], did not play a crucial role.

This changed at the end of the 1990s, when progress in laser cooling of atoms allowed the realization of frozen Rydberg gases[17,18], in which thermal motion is negligible over the timescales where interactions take place. Soon after, it was proposed that the strong interactions between Rydberg atoms could be harnessed to implement fast and robust quantum gates between neutral atoms[19,20]. The key ingredient for this implementation is the so-called Rydberg blockade (Box 1), where the interaction prevents the simultaneous Rydberg excitation of two nearby atoms. This allows for conditional logic, as the excitation of a second atom is governed by the excitation of a first one[21].

However, at the time, the control of neutral atoms at the individual level was still in its infancy[22], and only a few groups took up the challenge to demonstrate the Rydberg blockade between individually controlled atoms. This was finally achieved in 2009[23–26]. In the meantime, many groups had observed clear effects of the Rydberg blockade in large ensembles of atoms without individual control (see ref. [27] and references therein). One soon realized that the theoretical description of these systems naturally mapped onto that of the quantum Ising model[28–32], one of the simplest models used to describe quantum magnetism. This suggested that systems of neutral atoms in the Rydberg blockade regime could be used for quantum simulation, provided individual control of a large number of atoms was available.

In parallel, the progress in the manipulation and detection of individual neutral atoms has made tremendous progress, either by using quantum gas microscopes[33,34] or by creating arrays of optical tweezers[35–38]. Combined with Rydberg excitation to induce controllable interactions between the atoms, this provides an almost ideal platform to realize quantum spin models, as we will see below.

Arrays of individual atoms

The first experimental platform that allowed the control of ordered assemblies of neutral atoms at the single-particle level became available in 2010 and is the quantum gas microscope[39] (Fig. 1a). This 'top-down' approach relies on the loading of a two-dimensional ultracold atom cloud, typically a Bose–Einstein condensate—although fermions can also be used—into an optical lattice, the periodic optical potential obtained by interfering several laser beams. Atoms can tunnel between neighbouring sites of the lattice, and when the on-site contact interaction between the atoms overcomes the kinetic energy given by the tunnelling rate, the system undergoes a superfluid-to-Mott-insulator transition[40]. Deep in the Mott phase, the system is characterized by a fixed number of atoms per site, which can be exactly one for an appropriate choice of parameters. To obtain single-site resolution when imaging the atomic fluorescence, a high-numerical-aperture microscope objective is required, as two neighbouring sites are separated by typically

The strong interactions between atoms excited to a Rydberg state can be exploited to suppress the simultaneous excitation of two atoms and to generate entangled states, in a regime called Rydberg blockade. Consider a resonant laser field coherently coupling the ground state $|g\rangle$ and a given Rydberg state $|r\rangle$, with a Rabi frequency Ω (panel a). In the case of two atoms separated by a distance R (panel b), the doubly excited state $|rr\rangle$ is shifted in energy by the quantity C_6/R^6 due to the van der Waals interaction with C_6 being the interaction coefficient (all the other pair states have an energy nearly independent of R). We assume that the blockade condition $\hbar\Omega \ll C_6/R^6$ is fulfilled, that is, $R \ll R_b$ where the blockade radius is defined by $R_b = (C_6/\hbar\Omega)^{1/6}$. Then, starting from the ground state $|gg\rangle$, the system evolves to the collective state $|\psi_+\rangle = (|gr\rangle + |rg\rangle)\sqrt{2}$ with a coupling $\sqrt{2}\Omega$. The coupling to $|rr\rangle$ is now non-resonant and thus suppressed. This leads to a collective Rabi oscillation at the frequency $\sqrt{2}\Omega$ between $|gg\rangle$ and the entangled state $|\psi_+\rangle$.

The above considerations can be extended to an ensemble of N atoms all included within a blockade volume. In this case, at most one Rydberg excitation is possible, leading to collective Rabi oscillations with an enhanced frequency $\sqrt{N}\Omega$ between the collective ground state $|g\dots g\rangle$ and the entangled state $\sum |g\dots g r_i g\dots g\rangle/\sqrt{N}$ where the Rydberg excitation is shared among all the atoms. In the case of a system whose size is larger than the blockade radius (panel c), several Rydberg atoms can be excited, but their positions will be strongly correlated due to the blockade constraint, giving rise to complex many-body dynamics.
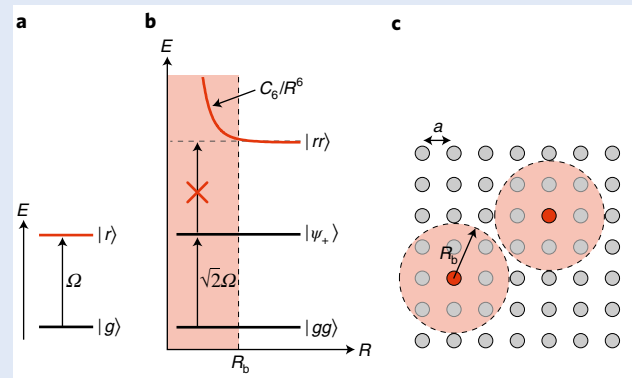
The Rydberg blockade. a, The ground and Rydberg states $|g\rangle$ and $|r\rangle$ are coupled by a resonant laser with Rabi frequency Ω. **b**, For two atoms separated by a distance $R < R_b$, the collective ground state $|gg\rangle$ is coupled only to $|\psi_+\rangle = (|gr\rangle + |rg\rangle)/\sqrt{2}$, but not to $|rr\rangle$, which is shifted out of resonance by the van der Waals interaction U_{vdW}. **c**, In a large ensemble of atoms, for example a regular array with spacing a, an atom excited in $|r\rangle$ (red dot) prevents the excitation of all the atoms contained in a sphere of radius R_b.

500 nm (refs. [33,34]). In this way, one realizes two-dimensional square arrays of up to a few hundred single atoms, with filling fractions that can exceed 95%. Individual control of the atoms can be achieved by applying local light shifts tailored with a spatial light modulator (SLM) such as a digital micromirror device[41].

More recently, a novel, 'bottom-up' platform has emerged based on arrays of optical tweezers (Fig. 1b). Trapping of a single laser-cooled atom in a tightly focused dipole trap, or optical tweezers, was demonstrated as early as 2001[22]. An optical dipole trap with a tight focus of about 1 μm is immersed in a magneto-optical trap (MOT). In the course of its random motion, an atom from
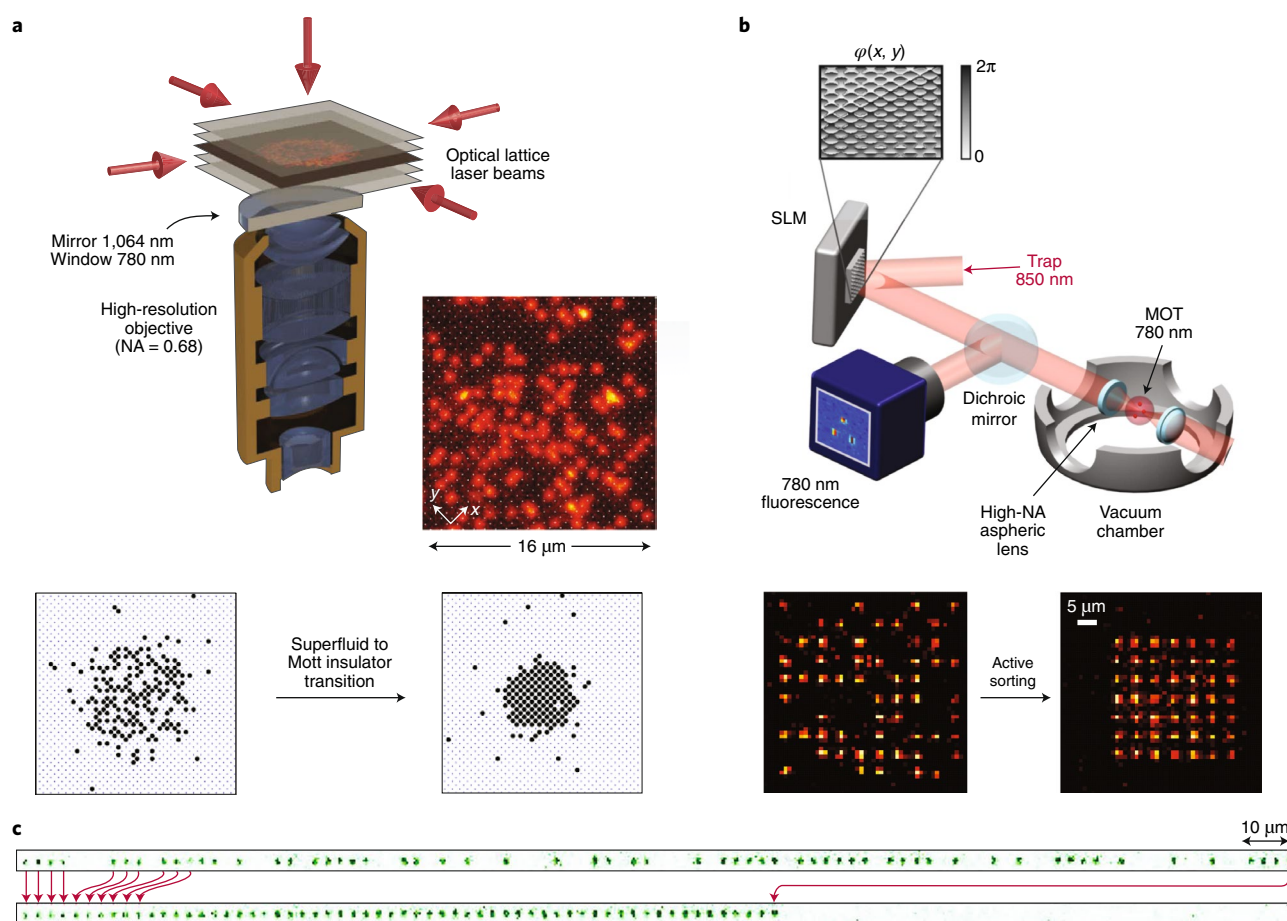
Fig. 1 | Experimental platforms for realizing arrays of individually controlled neutral atoms. a, In a quantum gas microscope, a high-numerical-aperture (NA) objective is used to observe the fluorescence of ultracold atoms trapped in an optical lattice obtained by interfering several laser beams. To achieve a filling of exactly one atom per site, one drives the superfluid-to-Mott-insulator transition[34]. **b**, In the tweezer array platform, an SLM imprints an appropriate phase on a trapping beam before focusing with a high-NA lens, resulting in arrays of traps with almost arbitrary geometries[35]. Single, laser-cooled atoms are loaded in the optical tweezers from a magneto-optical trap, resulting in a random loading array at half filling, which can be actively reordered into a target array using a moving optical tweezers[37]. Bottom: single shot fluorescence image of an array of traps before and after assembly. **c**, Alternatively, in one dimension, the tweezers can be generated using an acousto-optic deflector fed with multiple radio-frequency tones, which allows rearrangment of the atoms in a single step[38]. Panels adapted from: **a**, ref. [34], Springer Nature Ltd; **b**, top, ref. [35] under a Creative Commons licence (https://creativecommons.org/licenses/by/3.0/); **b**, bottom, ref. [37], AAAS; **c**, ref. [38], AAAS.

the MOT cloud enters the optical tweezers and gets trapped there. Since it is still under the illumination of the near-resonant MOT beams, it continuously scatters fluorescence light, which can be collected on a sensitive camera, thus signalling the presence of an atom in the tweezers. If now a second atom enters the trap, very fast light-assisted collisions give rise to the almost immediate loss of both atoms, and the tweezers are empty again. Therefore the number of atoms in the microtrap is either zero or one: this is a single-atom source, albeit non-deterministic since one cannot predict when the trap is occupied. The occupation probability is $p \sim 1/2$, as the same random event—namely an atom randomly entering the trap—induces the transitions either from one to zero atoms or from zero to one atom.

The next step is to produce arrays of microtraps. One method relies on an SLM[35,42], which imprints an appropriate phase pattern on the trapping beam before focusing, thus allowing the realization of almost arbitrary arrays of traps in the focal plane of the objective. Other methods use arrays of microlenses[43,44] or interference techniques[45]. However, for a long time, the stochastic loading of microtraps limited the use of this platform to just a few atoms, since the probability of having all N traps simultaneously filled decreases as $1/2^N$.

Careful engineering of the light-assisted collisions to lose just one atom of the pair[46,47] was shown to enhance p to values up to ~0.9, but the probability p^N of an N-trap array to be defect-free still decreases very quickly with N.

This problem was circumvented simultaneously in 2016 by three groups. The idea is to start from a large array with $2N$ traps, load it randomly with ~N atoms, take an image of this configuration, and finally actively sort the atoms into an ordered, target configuration[48]. This was achieved by two methods. In the first method, loaded tweezers are dynamically moved using acousto-optic deflectors to assemble one-dimensional chains[38] (Fig. 1c) as well as two-dimensional[49] and three-dimensional[36] arrays by slowly varying the phase pattern of the SLM creating the array. In the second method, atoms are moved one at a time using moving optical tweezers to catch and release atoms within a fixed two-dimensional array produced by an SLM[37] or microlenses[50]. More recently, the latter technique was extended to the assembly of three-dimensional arrays[51]. The assembly approach offers a fast repetition rate of the experiment (a few per second), filling fractions in excess of 98% even in large arrays and a great flexibility in geometry; the number of atoms reached so far is around 100 atoms. This sorting of atoms has also

Box 2 | Interactions between Rydberg atoms

Two atoms separated by a distance R much larger than the size of the electronic wavefunction interact mainly via the electric dipole–dipole Hamiltonian $\hat{V}_{dd} \sim \hat{d}_1 \hat{d}_2 / (4\pi\varepsilon_0 R^3)$ where $\hat{d}_i$ is the electric dipole moment of atom i and ε_0 the permittivity of a vacuum. The effect of this Hamiltonian on a pair of Rydberg atoms depends on how the pair is prepared.

In the most common case, the two atoms are excited in the same Rydberg level, for instance $|nS\rangle$. In this case, $\hat{V}_{dd}$ has no effect at first order in perturbation theory, as an atomic state has a vanishing average electric dipole moment. The effect of the interaction is thus of second order: the pair state $|nS, nS\rangle$ is coupled, via $\hat{V}_{dd}$, to other pair states of opposite parity, with a matrix element $V \propto d_1 d_2 / R^3$, where the energy of those states differ from that of $|nS, nS\rangle$ by a quantity Δ (panel a). This gives rise to a van der Waals shift of the considered pair state $|nS, nS\rangle$ scaling as $V^2/\Delta \propto C_6/R^6$ (ref. [112]). The C_6 coefficient is on the order of d^4/Δ, and thus scales roughly as n^{11} since $d \sim n^2$ and $\Delta \sim n^{-3}$. The dependence on the distance of the van der Waals interaction was directly measured for the cleanest system of a pair of single atoms at controlled positions in ref. [113], as was its angular dependence in ref. [114].

The van der Waals interaction between two Rydberg atoms is huge: it can reach tens of megahertz for atomic separations of several micrometres. However, Rydberg states have a lifetime on the order of a few hundreds of microseconds. To reach much

longer lifetimes, at the expense of reducing the interaction strength, the idea of Rydberg dressing has been proposed[75–79]. It consists of driving off-resonantly the transition from the ground to the Rydberg state, in a regime where the Rabi frequency is smaller than the detuning. The Rydberg state population remains negligible, but the ground state being weakly admixed with the Rydberg state, a pair of ground-state atoms acquire sizable interactions, with a long-distance tail decaying as $1/R^6$ beyond the Rydberg blockade radius, and a flat-top interaction at shorter distances. Panel b shows this soft-core potential, measured on a pair of single atoms trapped in optical tweezers, for two different detunings of the dressing laser[60].

In contrast, when the two atoms are prepared in two different, dipole-coupled Rydberg states, such as $|nS\rangle$ and $|nP\rangle$, the pair state $|nS, nP\rangle$ is directly coupled to the same-energy state $|nP, nS\rangle$ by $\hat{V}_{dd}$ (panel c). This gives rise to new eigenstates $|nS, nP\rangle \pm |nP, nS\rangle$ with energies $\pm C_3/R^3$. A pair of atoms initially prepared in $|nS, nP\rangle$ will coherently evolve into $|nP, nS\rangle$ and back, with a 'flip-flop' oscillation frequency $\propto R^{-3}$ (panel c). Moreover the interaction is anisotropic, varying as $1 - 3\cos^2\Theta$ with Θ the angle between the internuclear axis and the quantization axis (inset of panel c).

Finally, online calculators are now available to compute the interactions in all regimes, including in the presence of external electric and magnetic fields[55,56].
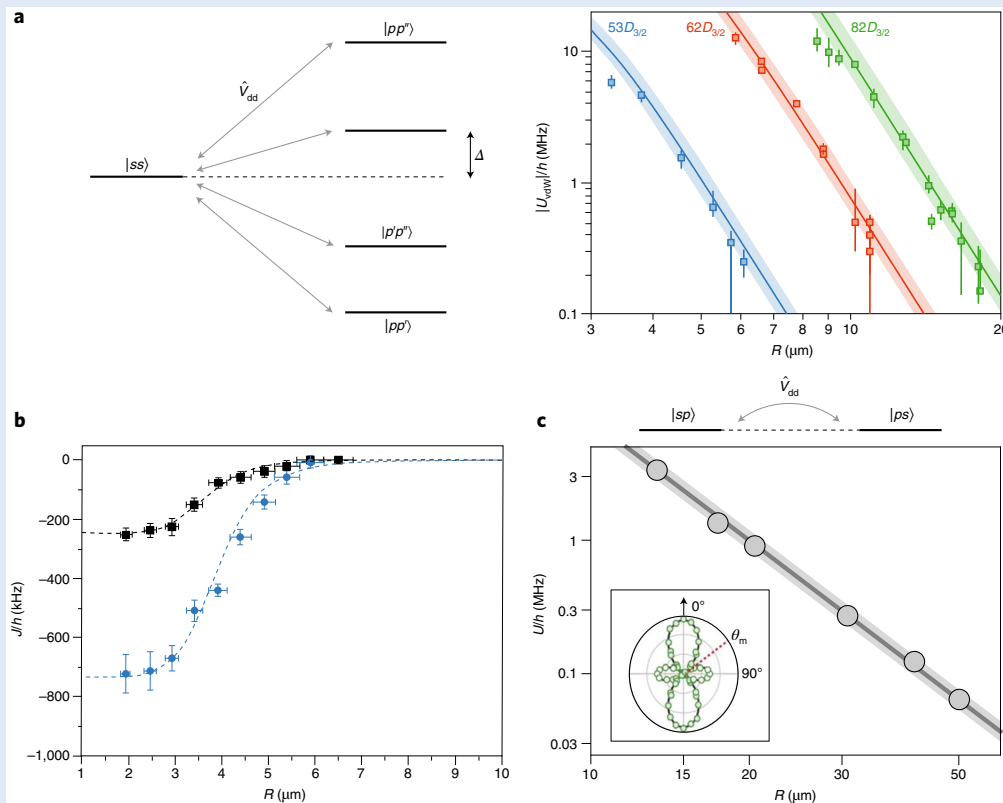
Interactions between Rydberg atoms. a, The van der Waals interaction between two identical Rydberg states, for instance, $|nS\rangle$ states, arises due to non-resonant dipolar interactions with other dipole-coupled Rydberg states. The C_6 coefficient varies extremely quickly with the principal quantum number n, as illustrated by this measurement for two atoms separated by R, excited to nD states[113], in agreement with ab initio calculations (solid lines). **b**, Soft-core potential between Rydberg dressed atoms, measured for a pair of single atoms, as a function of the atomic separation[61]. **c**, The resonant dipole–dipole interaction U arises when two atoms are in different, dipole-coupled Rydberg states, such as $|nS\rangle$ and $|n'P\rangle$. It varies as C_3/R^3 with the distance[89], with the angular dependence $C_3 \propto 1 - 3\cos^2\theta$ typical of the dipole–dipole interaction as revealed by the polar plot (inset). The interaction vanishes at the angle θ_m. Panels adapted from: **a**, ref. [113], APS; **b**, ref. [61], Springer Nature Ltd; **c**, ref. [89] under a Creative Commons licence (https://creativecommons.org/licenses/by/3.0/); **c**, inset, ref. [93], AAAS.

been applied in two and three dimensions in optical lattices with large spacing between sites[52,53].

Mapping Rydberg states onto spin systems

The large electric dipole moment of atoms excited to Rydberg states leads to strong dipole–dipole interactions between them[54–56], even for atoms separated by micrometre-large distances as in the lattices and arrays described above. Two types of interaction naturally occur between two Rydberg atoms (Box 2). In the context of quantum simulation, this leads to a mapping onto different spin models.

Let us consider first the case where the two atoms are placed in the same Rydberg state. There, the dipole–dipole interaction leads to the van der Waals interaction, which induces an energy shift of the pair state $|rr\rangle$ scaling as C_6/R^6, with R the atom separation (Box 2). This shift occurs only when both atoms are excited to the Rydberg state. If we now map the ground and Rydberg states $|g\rangle$ and $|r\rangle$ of each atom onto a spin-1/2 model following $|\downarrow\rangle = |g\rangle$ and $|\uparrow\rangle = |r\rangle$, the Hamiltonian of an ensemble of atoms driven by a coherent laser (Rabi frequency Ω, frequency detuning δ) is[28]

$$H = \frac{\hbar\Omega}{2}\sum_i \sigma_x^i - \hbar\delta\sum_i n_i + \sum_{i<j} V_{ij} n_i n_j, \text{ with } V_{ij} = \frac{C_6}{R_{ij}^6} \quad (1)$$

Here $\hbar$ is the reduced Planck's constant, n_i is the operator counting the number of Rydberg excitations at site i, and σ_x is the usual Pauli matrix. As n_i is related to the σ_z Pauli matrix by $n_i = (\sigma_z^i + 1)/2$, equation (1) has the form of the quantum Ising model, with a transverse field $B_\perp \propto \Omega$, a longitudinal field $B_\parallel \propto -\delta$ and Ising couplings J_{ij} decaying as $1/R_{ij}^6$ with distance. In practice, for the alkali atoms used so far, the laser excitation leading to the Rabi frequency Ω is often achieved on a two-photon transition, with one of the lasers in the infrared and the other one in the blue, far-detuned with respect to an intermediate state to avoid spontaneous emission[57,58]. In this way, the excitation is coherent to a good approximation. The Hamiltonian of equation (1) assumes that the excitation laser covers uniformly the atomic array, but owing to the single-site addressability, the detunings and Rabi frequency can be made site dependent by adding local laser control[59]. Finally, it is also possible to realize the quantum Ising model by using a technique called Rydberg dressing and encoding the two spin states in ground-state long-lived levels[60]. In this case, the couplings J_{ij} have a soft-core spatial dependence (Box 2).

We now consider the second case where the atoms are prepared in two different Rydberg states that are dipole-coupled, such as $|nS\rangle$ and $|nP\rangle$, separated by a transition frequency typically in the 10 GHz range. There, the dipole–dipole interaction gives rise to a coherent exchange of the internal states of the atoms and the interaction potential scales as C_3/R^3. The mapping onto a spin-1/2 model is then $|\downarrow\rangle = |nS\rangle$ and $|\uparrow\rangle = |nP\rangle$. Microwave radiation can be used to manipulate the spin and thus acts as an external magnetic field.

$$H = \frac{\hbar\Omega_{\mu w}}{2}\sum_i \sigma_x^i - \frac{\hbar\delta_{\mu w}}{2}\sum_i \sigma_z^i + \sum_{i\neq j}\frac{C_3}{R_{ij}^3}\left(\sigma_+^i\sigma_-^j + \sigma_-^i\sigma_+^j\right) \quad (2)$$

which is the XY spin Hamiltonian with transverse and longitudinal fields given by the Rabi frequency $\Omega_{\mu w}$ and the detuning $\delta_{\mu w}$ of the microwave field.

Both the Ising and the XY Hamiltonians have been extensively studied over the past 60 years in various contexts, such as magnetism and excitation transport. However, many important open questions remain the subject of active research, such as the nature of the phase diagram when the spins are placed in arrays featuring geometrical frustration, the dynamics of the system after the sudden variation of parameters of the Hamiltonian, the role of disorder in the couplings, their combination with situations where topology plays a role, and so on. Furthermore, as explained in the introduction,

many combinatorial optimization problems can be mapped onto spin models[7], and their interest thus extends beyond the traditional realm of many-body physics. All these questions can be studied using the Rydberg platforms described here, as we now show.

Quantum simulation of the Ising model

To study many-body systems experimentally one can, for example, vary suddenly one parameter of the Hamiltonian and study the resulting dynamics of the closed many-body system. One can also prepare the ground state using an adiabatic variation of the parameters of the Hamiltonian, and study its properties. The experiments performed on Rydberg quantum simulators in the Ising model regime used these two approaches.

Let us first discuss qualitatively the generic phase diagram of the quantum Ising model described by equation (1), at zero temperature and for spins placed on a chain or on two-dimensional square arrays. We first consider the case of nearest-neighbour couplings only ($V_{i,i+1} = V$ and 0 otherwise) and assume $V > 0$, so that the interactions favour antiferromagnetic ordering. The phase diagram consists of two regions, a paramagnetic and an antiferromagnetic one, separated by a quantum phase transition, as represented in Fig. 2a. Two limiting cases are easy to understand: for $\Omega, \delta \gg V$, the ground state is paramagnetic, that is, the spins align along the effective magnetic field; for $\Omega = 0$, the phase results from the minimization of the energy of the classical configuration. When we relax the constraint of nearest-neighbour couplings only (as is the case for a van der Waals interaction), the phase diagram exhibits several phases around the line separating the paramagnetic from the antiferromagnetic phases. For example, on a chain, if $V_{i,i+1}, V_{i,i+2} \gg \delta \gg \Omega \gg V_{i,i+3}$, the ground state corresponds to one excitation separated by two ground-state atoms (Z_3 symmetry). This situation corresponds to a blockade radius $R_b = 2a$, with a the spacing between atoms. Similarly, $V_{i,i+1}, V_{i,i+2}, V_{i,i+3} \gg \delta \gg \Omega \gg V_{i,i+4}$ leads to a phase with Z_4-symmetry, and so on. By controlling the detuning δ and Rabi frequency Ω, one can explore the phase diagram of this Ising model.

The sudden variation of a parameter in the Hamiltonian (also called a quench) is the easiest method to implement experimentally. In the case of the Rydberg platform, all the experiments realized so far suddenly applied the Rydberg excitation laser mimicking the transverse magnetic field, usually at resonance ($\delta = 0$), after having prepared the atoms in their ground state, corresponding to spin $|\downarrow\rangle$. They then measure two quantities relevant to the study of spin systems: first, the average magnetization, namely, the average number of atoms excited to the Rydberg states, or equivalently in the spin state $|\uparrow\rangle$; second, the spin–spin correlation function, which is the probability of finding a Rydberg excitation at site j when one is already present at site i. The measurement of this correlation function is only made possible owing to the fact that the quantum gas microscope and the tweezer array platforms allow for single-site readout of the atomic state.

The first implementation of this method was reported in ref. [61], and made use of a quantum gas microscope. The system was operated in a regime with the blockade radius R_b much larger than the intersite distance $a \sim 500$ nm. The effect of the blockade was observed by the fact that the emergent Rydberg excitations were separated typically by a distance R_b. The dynamics of the appearance of the excitation could be followed and compared with the theoretical prediction of the Ising model. Later, the $\sqrt{N}$ enhanced coupling for an ensemble of up to 200 atoms all within a blockade radius was also demonstrated[62].

The case $R_b \gg a$, as explored in refs. [61,62], is an extreme situation where the interaction dominates all the energy scales in the problem. It is also interesting to explore the case where the interaction energy between neighbouring atoms is on the order of the energy scale associated with the transverse field, that is, operating at $R_b \sim a$. The tweezer arrays are naturally in this regime. As an example,
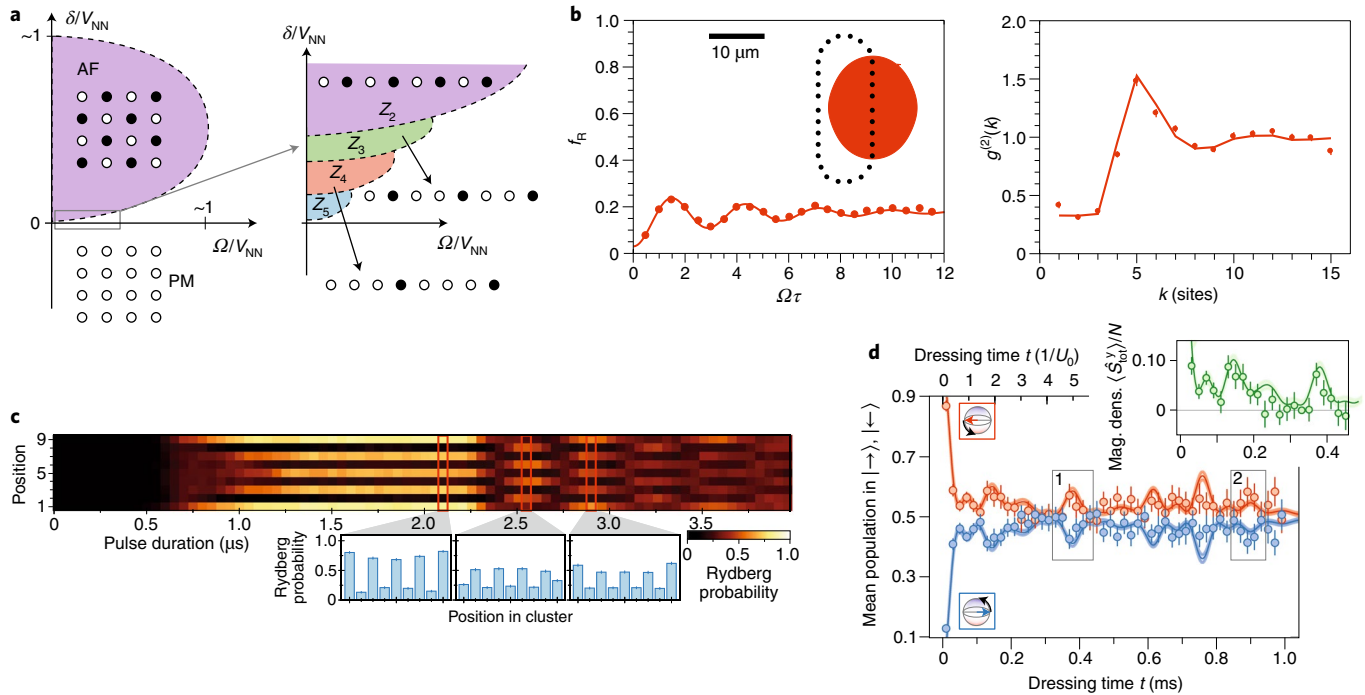
Fig. 2 | Quantum quench experiments for the Ising model. a, Schematic phase diagram of the quantum Ising model for a two-dimensional square or a one-dimensional chain of atoms interacting via the van der Waals interaction, showing the paramagnetic (PM) and antiferromagnetic (AF) phases. Here $V_{NN} = C_6/a^6$, with a the spacing between atoms (we take $C_6 > 0$). The right side is a zoom of the phase diagram around the critical point ($\Omega = 0$, $\delta = 0$), for a one-dimensional chain. **b**, Quantum quench in a one-dimensional Ising magnet with periodic boundary conditions, starting with all atoms in $|\downarrow\rangle$, for $R_b/a \simeq 4$ (ref. [63]). The dotted area represents the chain configuration and the filled oval represents the blockade volume. The magnetization of the chain (left), corresponding to the fraction f_R of atoms excited to the Rydberg state, and the spin–spin correlation function $g^{(2)}(k)$ (right), with k being the spin separation, show clear effects of the Rydberg blockade. The solid lines are simulations of the Schrödinger equation without any adjustable parameter. **c**, In ref. [67], a quasi-adiabatic sweep was used, in the regime $R_b/a \simeq 1.5$, to prepare an 'antiferromagnet' state $|\uparrow\downarrow\uparrow\downarrow\cdots\rangle$. This state was then suddenly quenched (at 2.2 μs) by driving it on resonance, resulting in surprisingly long-lived collective oscillations between $|\uparrow\downarrow\uparrow\downarrow\cdots\rangle$ and $|\downarrow\uparrow\downarrow\uparrow\cdots\rangle$. Insets: Rydberg excitations along the line for various pulse durations. **d**, Rydberg dressing can also be used to study quenches of Ising magnets. In ref. [80], a chain of ten atoms all initially prepared in $|\leftarrow\rangle = (|\uparrow\rangle + |\downarrow\rangle)/\sqrt{2}$ was suddenly subjected to the Ising Hamiltonian, giving rise to a dynamical evolution showing collapse and revivals of the magnetization along x. Inset: initial dynamics of the mean transverse magnetization density. Panels adapted from: **b**, ref. [63], Springer Nature Ltd; **c**, ref. [67], Springer Nature Ltd; **d**, ref. [80] under a Creative Commons licence (https://creativecommons.org/licenses/by/3.0/).

a one-dimensional chain of ~20 atoms with periodic boundary conditions (Fig. 2b) was explored[63]. The dynamics observed after suddenly turning on the excitation laser and the pair correlation functions measured in the experiment were compared with the solution of the Schrödinger equation for this many-body system, including all the experimental imperfections. The agreement with the data was very good, and this theory–experiment comparison can be considered as a benchmark for this Rydberg quantum simulator in a regime where ab initio calculations are still possible. In particular, the appearance of a steady-state regime for the magnetization at long time results from the beating of all the eigenfrequencies of this interacting system. The behaviour of the pair correlation function (also observed in two dimensions in ref. [61]) with its suppression at short distance and its oscillatory behaviour at larger distance is reminiscent of the pair correlation function of a liquid of hard rods with an effective particle size of R_b. The quench experiment in a 7×7 array was repeated in ref. [64]. To draw a comparison between the observed dynamics and theory, approximations had to be made as the number of particles involved in this case is too large to allow for ab initio calculations. These studies have been refined in refs. [65,66], where the appearance of a steady state at long evolution times was considered as an evidence of thermalization of the system.

Finally an out-of-equilibrium situation was also studied in ref. [67]. But in contrast to the experiments described above, the ground state of the many-body system was obtained from an adiabatic preparation detailed below. By suddenly changing the detuning of the laser to cross a quantum phase transition, non-trivial dynamics was observed with long-lived collective oscillations that have been modelled (Fig. 2c).

A second method to study many-body systems consists of preparing the ground state of the system. To do so, one starts from the state where all atoms are prepared in their ground state: $|\psi_{ini}\rangle = |ggg\ldots\rangle$. By sweeping the Rabi frequency $\Omega(t)$ and detuning $\delta(t)$ on a timescale that is long with respect to the inverse of the energy gap with the first excited state, the system is driven adiabatically in the ground state of the interacting system for a given final value of Ω and δ. This approach, initially suggested in ref. [68], was first demonstrated in the regime $R_b \gg a$ (ref. [69]): there, a controlled number of excitations separated by R_b in one and two dimensions was observed, a situation reminiscent of a crystal (Fig. 3a).

The regime $R_b \sim a$ was then explored in three experiments. The one-dimensional case with up to 51 atoms was investigated in ref. [67] (Fig. 3b). Several phases with Z_n symmetries were found to be accessible by varying the ratio R_b/a between 2 and 4. The two-dimensional case was explored in refs. [70,71] using atoms in tweezer arrays and in optical lattices, respectively (Fig. 3d). Both observed the appearance of antiferromagnetic correlations. Reference[70] also studied the propagation of these correlations during the adiabatic ramp of the parameters. Let us note that this adiabatic approach becomes
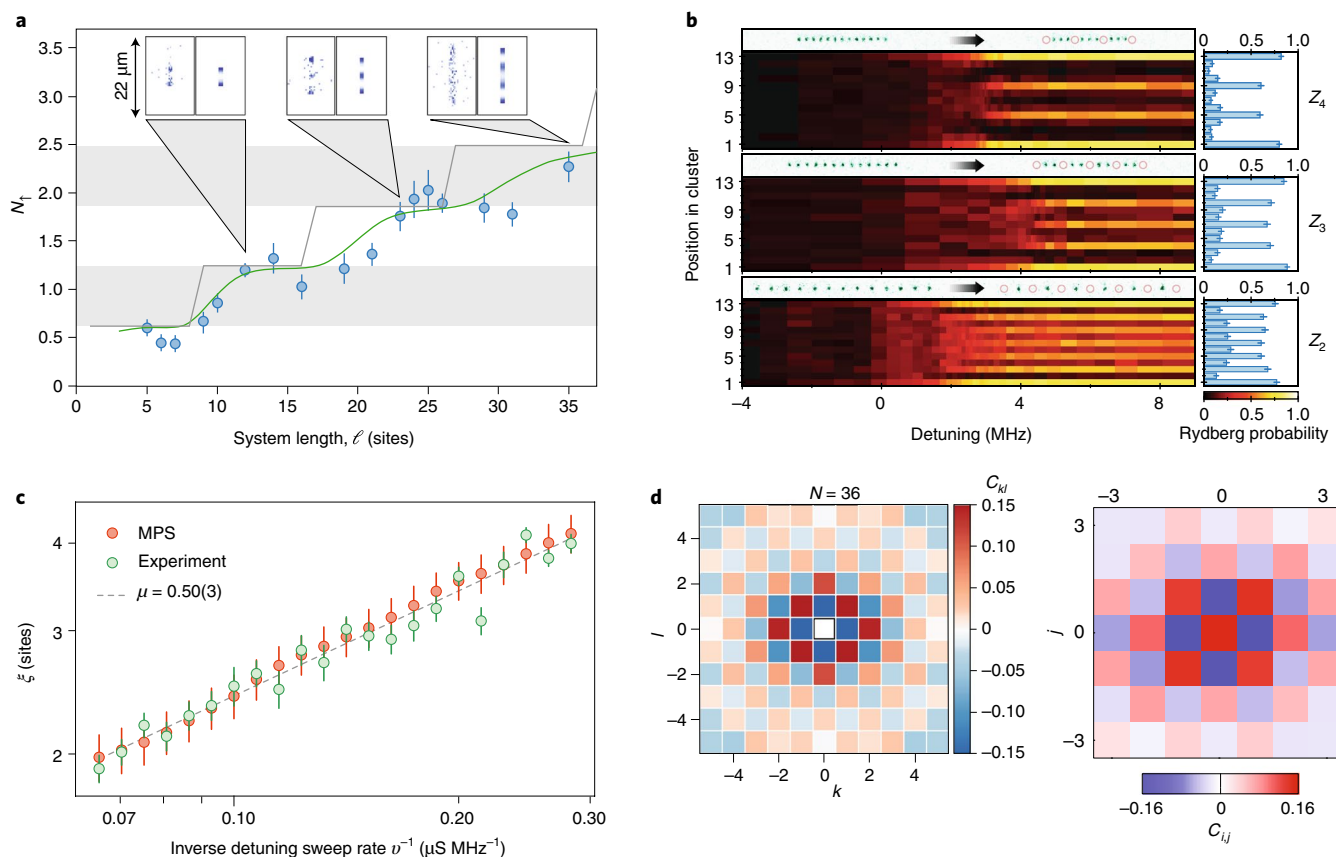
Fig. 3 | Quasi-adiabatic sweeps experiments for the Ising model. a, 'Crystallization' of Rydberg excitations in a quasi-one-dimensional chain, in a regime where the blockade radius is much larger than the lattice spacing a. When the chain length is increased, the number of excitations increases in a step-like manner[69]. Insets: measured spatial distribution of Rydberg excitations (left) and corresponding theory (right) for various system lengths. **b**, Adiabatic preparation of the ground state of a 13-atom chain for various values of R_b/a, giving an excitation every second site, every third site or every fourth site, corresponding to different ordered phases Z_n of the system[67]. **c**, Antiferromagnetic correlation length ξ obtained in a chain of 51 atoms as a function of the detuning sweep rate[72]. The slope gives access to the critical exponents characterizing the quantum phase transition. MPS, matrix product state simulation. **d**, Antiferromagnetic spin–spin correlation function in two-dimensional arrays of atoms after adiabatic preparation for the experiment in ref. [70] (left) and ref. [71] (right). Panels adapted from: **a**, ref. [69], AAAS; **b**, ref. [67], Springer Nature Ltd; **c**, ref. [72], Springer Nature Ltd; **d**, ref. [70] (left) and ref. [71] (right) under a Creative Commons licence (https://creativecommons.org/licenses/by/3.0/).

harder and harder as the system size increases, as the energy gap vanishes at the quantum phase transition.

Of course, the transition between the quenched and adiabatic regimes is continuous. Reference [72] studied what happens at the quantum phase transition when the parameters are varied at different rates. It was found that if the ramp is too fast, defects with respect to the ideal Z_n symmetry appear. These defects can be studied according to a model introduced by Kibble and Zurek in the 1980s[73,74]. In particular, the correlation length obtained as a function of the speed at which the parameters are ramped follows a universal law with a critical exponent that can be extracted from the experiment (Fig. 3c). An experimental value was found to be in excellent agreement with the theoretical prediction from the Ising model, nicely illustrating that synthetic quantum systems can be used to measure the properties of quantum phase transitions with high precision.

As pointed out at the beginning of this Review, Rydberg atoms have lifetimes in the hundreds of microseconds, which is long enough to observe interaction-driven dynamics. However, revivals in the dynamics, occurring at long times for large systems, may be hard to observe, as the atoms decay to their ground states before the revival occurs. The Rydberg dressing introduced earlier was proposed as an alternative to circumvent this problem[75–79]. First experiments

in this direction were performed in refs. [80,81]. There, the spin is encoded in two hyperfine ground states of rubidium atoms. The atoms arranged along a chain (containing around ten atoms) are initially all prepared in a superposition state $\propto |\uparrow\rangle + |\downarrow\rangle$. A laser is then switched on to admix the state $|\uparrow\rangle$ with a Rydberg state $|r\rangle$, thus making the atoms interact. The system evolves under the influence of the interactions. After some time, the laser is switched off and the state of each atom is read out. One can then compute the average magnetization and the correlations. As shown in Fig. 2d, revivals of the magnetization were observed. Although this result is very encouraging as it shows the potential of Rydberg dressing, it remains unclear at present how large the system sizes can be, as unwanted losses appear during the dressing when the number of atoms increases[81–83].

Quantum simulation using resonant exchange interactions

As explained above, the resonant dipole–dipole interaction between two Rydberg states naturally realizes the XY spin-1/2 model. Besides its interest for the study of quantum magnetism, this model is also useful to describe transport properties in many situations. Let us think, for example, about a chain of spin-1/2 particles all prepared in their state $|\downarrow\rangle$ and able to interact by the XY interaction. If one now flips the spin of one of them to $|\uparrow\rangle$, this spin excitation will
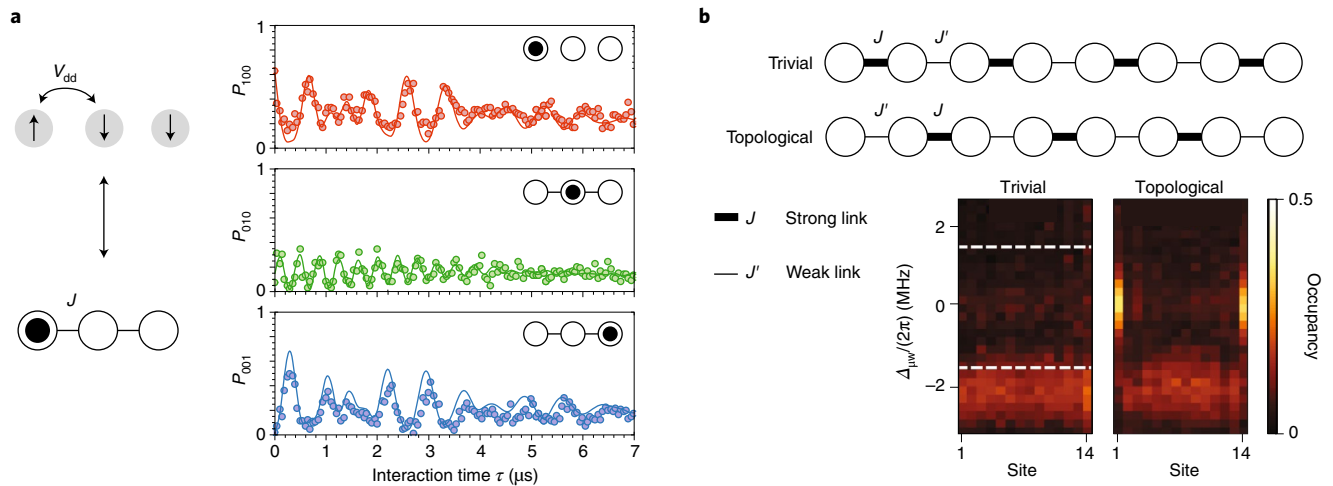
Fig. 4 | Quantum simulation of the XY model. a, Left: mapping between the XY model and the propagation of a particle from one site to another in a chain. Right: illustration in a chain of three atoms, where the initial state is |*PSS*⟩. Evolution of the probability that the particle '*P*' is on the left, centre or right site, as a function of time. One observes quasi-revivals due to long-range couplings. **b**, Implementation of the SSH model using Rydberg atoms. The model consists of a chain with alternating strong and weak couplings between neighbouring sites. A finite chain of an even number of sites exists in two different configurations (called normal or topological), with the weak or strong link at the edges. Bottom: microwave spectroscopy of the SSH model implemented on a chain of Rydberg atoms: probability of exciting the atoms from Rydberg state nS to nP as a function of the frequency $\Delta_{\mu w}$ of the microwave, for different positions in the chain. The topological configuration features two states at zero energy, corresponding to atoms located at the two edges of the chain. Panels adapted from: **a**, ref. [88] under a Creative Commons licence (https://creativecommons.org/licenses/by/3.0/); **b**, ref. [92], AAAS.

propagate along the chain under the influence of the exchange inter-action, in the same way that a single particle can tunnel between neighbouring sites in a lattice. This transport of excitations driven by the resonant dipolar interaction is, for example, the process that takes place in photosynthesis, where the energy deposited by light in a light-harvesting cell is carried towards a reaction centre[84].

This example suggests using a different language to describe the transport of spin excitations under the influence of the resonant dipole interaction. Let us now view the |↓⟩ state as the absence of a particle (the 'vacuum'), and rename it |0⟩. The state |↑⟩ now corresponds to the presence of a particle, that we call |1⟩. In a chain, the state |0000…⟩ corresponds to no particle on any site, while, for example, |0100…⟩ indicates the situation where one particle is present on the second site of the chain. We can also consider the sit-uation where two excitations are present in the chain, for example, by preparing the state |0110…⟩. Importantly, these particles inter-act very strongly: as one atom cannot carry more than one excita-tion, it is not possible to find two particles on the same lattice site. Therefore, spin excitations behave as artificial particles with infinite on-site interactions—a hard-core constraint. It turns out that the spin excitations have the same commutation relations as those of bosons. Therefore, the problem of an ensemble of two-level Rydberg atoms interacting by the resonant dipole–dipole interaction can be equivalently mapped onto a spin-1/2 XY model or onto a system of hard-core bosons[85]. But one should keep in mind that the resonant dipolar interaction that drives the transport of an excitation leads to a single-particle problem when considering a single excitation. What makes the excitations interact is the fact that the atoms only have two levels, and not the fact that the atoms carrying the excita-tions interact.

The first experiments performed with Rydberg atoms in a laser-cooled gas were actually a study of the transport of excita-tions driven by the dipole–dipole interaction in a situation where the atoms' positions are frozen[17,18]. Since then, several experiments refined our understanding of the dynamics of the propagation in atomic ensembles with random positions[86,87]. The case where the atoms are placed in regular arrays with individual control has been

much less studied experimentally, and, so far, only two experiments have used the resonant dipole–dipole interaction to perform a quantum simulation.

One of them was a proof-of-principle experiment demonstrat-ing the propagation of a spin excitation in a chain of three atoms[88]. Preparing three atoms all in the same |nD⟩ Rydberg state, we flipped the state of the first one into a state |$n'P$⟩ and observed how the 'P' excitation moved in the chain. The results, shown in Fig. 4a, indicate that despite the simplicity of the situation, the dynamics is already non-trivial: this comes from the fact that the two energy scales in the problem, C_3/a^3 and $C_3/8a^3$, lead to three incommensurate eigen-values of the Hamiltonian.

The goal of the second experiment was to implement the Su–Schrieffer–Heeger (SSH) model, initially developed in the late 1970s to explain the conductivity of some organic polymers[89,90]. Its sim-plest setting consists of a one-dimensional chain of sites that are coupled by alternating strong and weak links and where an exci-tation can hop in the chain. Since then, the SSH model has been recognized as one of the simplest examples of a system exhibiting topological properties.

Let us consider the two configurations of a finite chain repre-sented in Fig. 4b: either the chain ends up with the strongest link J, or with the weakest one J'. One can show that in the first configura-tion, the single-particle spectrum consists of two bands with width J', separated by an energy gap $|J - J'|$. In contrast, in the second configuration, two states at zero energy appear in the middle of the gap, and correspond to states localized on the edges of the chain. The fact that they have zero energy is rather intuitive in the extreme case where $J' = 0$, as adding a particle on each edge does not cost energy. It turns out that this remains true even when $J' \neq 0$. The two configurations correspond to two different topological classes of the system: it is impossible to vary the ratio J/J' and continuously trans-form one configuration into the other without closing the gap[91].

Implementing this model in a chain of Rydberg atoms allows the study of both single-particle properties and the genuinely many-body properties arising from the hard-core constraint[92]. Microwave spec-troscopy was used to measure the single-particle energy spectrum

(Fig. 4). The many-body regime has been reached by preparing the ground state of the chain comprising $N/2$ excitations (where N is the number of sites), using an adiabatic preparation relying on slow sweeps of the amplitude and frequency of a microwave. The many-body ground state studied in the topological configuration was found to display a characteristic robustness with respect to the breaking of certain symmetries of the Hamiltonian. The prepared state is probably the first experimental realization of a type of topological order for bosons introduced in 2012[93], called symmetry-protected topological phases, which are the only topological orders that can exist in one dimension.

Perspectives

Finally, we discuss short- and longer-term perspectives on the use of Rydberg atoms for quantum simulation. The field is rapidly evolving, and here we merely identify a few emerging directions of research.

Obvious trends in the short term, on the technical side, are (1) to improve the fidelity of the simulations and (2) to scale up the number of atoms in the arrays. The first objective requires not only, at the single-particle level, understanding the limitations of the Rydberg excitation schemes[94] and overcoming them, for instance, using different schemes for the two-photon transitions[95], but also, at the two-atom level, optimizing the mapping of the complex level structure of interacting Rydberg atoms onto simple two-level systems[64]. In addition, the possibility to scale up the number of atoms to several hundreds is one of the crucial assets of Rydberg arrays when compared with other platforms. To do so, the recently demonstrated use of gray-molasses loading of optical tweezers[96] opens up exciting prospects as, for a given trap depth, the required optical power per trap is strongly reduced, and, at the same time, the loading probability p is significantly enhanced. Cryogenic platforms such as the ones recently developed for trapped ion chains[97] could help increase the atomic trapping lifetime and thus help in scaling up the number of atoms.

The second short-term prospect is the extension of the techniques that have so far been applied to alkali atoms to new atomic species with two valence electrons. Arrays of single strontium[98–100] and ytterbium[101] atoms have been reported recently. Although so far no quantum simulation has been performed with these novel systems, the richer internal structure of these species might allow new ways to manipulate, control and probe them[102,103].

A longer-term goal would consist of using arrays of circular Rydberg states for quantum simulation. Not only would they allow the implementation of more complex spin models, such as the Heisenberg Hamiltonian, in a more natural way, but also they may, with their much longer lifetimes, open up the possibility to study long-time dynamics with Rydberg quantum simulators[104].

Finally, one exciting prospect for Rydberg array quantum simulators is the fact that their applications may extend to a much broader class of problems than that of the mere implementation of spin Hamiltonians inspired by quantum magnetism, as they could be used to study optimization problems by quantum annealing[105,106]. While for general optimization problems Rydberg arrays may have limitations comparable to other platforms, they could be, for instance, particularly adapted to solving a classical combinatorial problem in graph theory, namely finding the maximum independent set of a graph[107].

A hybrid, closed-loop approach, combining a Rydberg quantum simulator with increased degree of control and a classical computer, could be used to implement variational quantum simulation. There, the quantum machine is used for efficiently generating many-body quantum states depending on a small number of variational parameters and measuring the average value of non-trivial observables, while classical hardware is used to optimize these parameters, making it possible to find in an iterative way, for example, the ground state of spin Hamiltonians that cannot be realized physically with the platform at hand[108]. This type of architecture blurs the distinction between programmable quantum simulators and noisy, intermediate-scale quantum computers[109], for which Rydberg atom arrays are also a promising platform[110,111].

References

1. Feynman, R. P. Simulating physics with computers. *Int. J. Theor. Phys.* **21**, 467–488 (1982).
2. Lloyd, S. Universal quantum simulators. *Science* **273**, 1073–1078 (1996).
3. Georgescu, I. M., Ashhab, S. & Nori, F. Quantum simulation. *Rev. Mod. Phys.* **86**, 153–185 (2014).
4. Giovannetti, V., Lloyd, S. & Maccone, L. Advances in quantum metrology. *Nat. Photon.* **5**, 222–229 (2011).
5. Nielsen, M. A. & Chuang, I. L. *Quantum Computation and Quantum Information* (Cambridge Univ. Press, 2010).
6. Preskill, J. Quantum computing and the entanglement frontier. Preprint at https://arxiv.org/abs/1203.5813 (2012).
7. Lucas, A. Ising formulations of many NP problems. *Front. Phys.* **2**, 5 (2014).
8. Blatt, R. & Roos, C. F. Quantum simulations with trapped ions. *Nat. Phys.* **8**, 277–284 (2012).
9. Bloch, I., Dalibard, J. & Nascimbène, S. Quantum simulations with ultracold quantum gases. *Nat. Phys.* **8**, 267–276 (2012).
10. Houck, A. A., Türeci, H. E. & Koch, J. On-chip quantum simulation with superconducting circuits. *Nat. Phys.* **8**, 292–299 (2012).
11. Aspuru-Guzik, A. & Walther, P. Photonic quantum simulators. *Nat. Phys.* **8**, 285–291 (2012).
12. Chang, D. E., Vuletić, V. & Lukin, M. D. Quantum nonlinear optics — photon by photon. *Nat. Photon.* **8**, 685–694 (2014).
13. Gallagher, T. F. *Rydberg Atoms* (Cambridge Univ. Press, 1994).
14. Sibalić, N. & Adams, C. S. *Rydberg Physics* (IOP, 2018); https://iopscience.iop.org/book/978-0-7503-1635-4.
15. Haroche, S. Controlling photons in a box and exploring the quantum to classical boundary. *Rev. Mod. Phys.* **85**, 1083–1102 (2013).
16. Raimond, J.-M., Vitrant, G. & Haroche, S. Spectral line broadening due to the interaction between very excited atoms: 'the dense Rydberg gas'. *J. Phys. B* **14**, L655–L660 (1981).
17. Anderson, W. R., Veale, J. R. & Gallagher, T. F. Resonant dipole-dipole energy transfer in a nearly frozen Rydberg gas. *Phys. Rev. Lett.* **80**, 249–252 (1998).
18. Mourachko, I. et al. Many-body effects in a frozen Rydberg gas. *Phys. Rev. Lett.* **80**, 253–256 (1998).
19. Jaksch, D., Cirac, J. I., Zoller, P., Côté, R. & Lukin, M. D. Fast quantum gates for neutral atoms. *Phys. Rev. Lett.* **85**, 2208–2211 (2000).
20. Lukin, M. D. et al. Dipole blockade and quantum information processing in mesoscopic atomic ensembles. *Phys. Rev. Lett.* **87**, 037901 (2001).
21. Saffman, M., Walker, T. G. & Mølmer, K. Quantum information with Rydberg atoms. *Rev. Mod. Phys.* **82**, 2313–2363 (2010).
22. Schlosser, N., Reymond, G., Protsenko, I. & Grangier, P. Sub-poissonian loading of single atoms in a microscopic dipole trap. *Nature* **411**, 1024–1027 (2001).
23. Urban, E. et al. Observation of Rydberg blockade between two atoms. *Nat. Phys.* **5**, 110–114 (2009).
24. Gaëtan, A. et al. Observation of collective excitation of two individual atoms in the Rydberg blockade regime. *Nat. Phys.* **5**, 115–118 (2009).
25. Wilk, T. et al. Entanglement of two individual neutral atoms using Rydberg blockade. *Phys. Rev. Lett.* **104**, 010502 (2010).
26. Isenhower, L. et al. Demonstration of a neutral atom controlled-NOT quantum gate. *Phys. Rev. Lett.* **104**, 010503 (2010).
27. Comparat, D. & Pillet, P. Dipole blockade in a cold Rydberg atomic sample. *J. Opt. Soc. Am. B* **27**, A208–A232 (2010).
28. Robicheaux, F. & Hernández, J. V. Many-body wave function in a dipole blockade configuration. *Phys. Rev. A* **72**, 063403 (2005).
29. Weimer, H., Löw, R., Pfau, T. & Büchler, H. P. Quantum critical behavior in strongly interacting Rydberg gases. *Phys. Rev. Lett.* **101**, 250601 (2010).
30. Weimer, H., Müller, M., Lesanovsky, I., Zoller, P. & Büchler, H. P. A Rydberg quantum simulator. *Nat. Phys.* **6**, 382–388 (2010).
31. Olmos, B., González-Férez, R. & Lesanovsky, I. Collective Rydberg excitations of an atomic gas confined in a ring lattice. *Phys. Rev. A* **79**, 043419 (2009).
32. Lesanovsky, I. Many-body spin interactions and the ground state of a dense Rydberg lattice gas. *Phys. Rev. Lett.* **106**, 025301 (2011).
33. Bakr, W. S. et al. Probing the superfluid-to-Mott insulator transition at the single-atom level. *Science* **329**, 547–550 (2010).

34. Sherson, J. F. et al. Single-atom-resolved fluorescence imaging of an atomic Mott insulator. *Nature* **467**, 68–72 (2010).
35. Nogrette, F. et al. Single-atom trapping in holographic 2D arrays of microtraps with arbitrary geometries. *Phys. Rev. X* **4**, 021034 (2014).
36. Lee, W., Kim, H. & Ahn, J. Three-dimensional rearrangement of single atoms using actively controlled optical microtraps. *Opt. Express* **24**, 9816–9825 (2016).
37. Barredo, D., de Léséleuc, S., Lienhard, V., Lahaye, T. & Browaeys, A. An atom-by-atom assembler of defect-free arbitrary two-dimensional atomic arrays. *Science* **354**, 1021–1023 (2016).
38. Endres, M. et al. Atom-by-atom assembly of defect-free one-dimensional cold atom arrays. *Science* **354**, 1024–1027 (2016).
39. Gross, C. & Bloch, I. Quantum simulation with ultra-cold atoms in optical lattices. *Science* **357**, 995–1001 (2017).
40. Greiner, M., Mandel, O., Esslinger, T., Hänsch, T. W. & Bloch, I. Quantum phase transition from a superfluid to a Mott insulator in a gas of ultracold atoms. *Nature* **415**, 39–44 (2002).
41. Weitenberg, C. et al. Single-spin addressing in an atomic Mott insulator. *Nature* **471**, 319–324 (2011).
42. Bergamini, S. et al. Holographic generation of micro-trap arrays for single atoms. *J. Opt. Soc. Am. B* **21**, 1889–1894 (2004).
43. Dumke, R. et al. Micro-optical realization of arrays of selectively addressable dipole traps: a scalable configuration for quantum computation with atomic qubits. *Phys. Rev. Lett.* **89**, 097903 (2002).
44. Schlosser, M. et al. Fast transport, atom sample splitting, and single-atom qubit supply in two-dimensional arrays of optical microtraps. *New J. Phys.* **14**, 123034 (2012).
45. Piotrowicz, M. J. et al. Two-dimensional lattice of blue-detuned atom traps using a projected Gaussian beam array. *Phys. Rev. A* **88**, 013420 (2013).
46. Grünzweig, T., Hilliard, A., McGovern, M. & Andersen, M. F. Near-deterministic preparation of a single atom in an optical microtrap. *Nat. Phys.* **6**, 951–954 (2010).
47. Lester, B. J., Luick, N., Kaufman, A. M., Reynolds, C. M. & Regal, C. A. Rapid production of uniformly filled arrays of neutral atoms. *Phys. Rev. Lett.* **115**, 073003 (2015).
48. Miroshnychenko, Y. et al. An atom sorting machine. *Nature* **442**, 151 (2007).
49. Kim, H. et al. In situ single-atom array synthesis using dynamic holographic optical tweezers. *Nat. Commun.* **7**, 13317 (2016).
50. Ohl de Mello, D. et al. Defect-free assembly of 2D clusters of more than 100 single-atom quantum systems. *Phys. Rev. Lett.* **122**, 203601 (2019).
51. Barredo, D., Lienhard, V., de Léséleuc, S., Lahaye, T. & Browaeys, A. Synthetic three-dimensional atomic structures assembled atom by atom. *Nature* **561**, 79–82 (2018).
52. Nelson, K. D., Xiao, L. & David, S. Weiss. Imaging single atoms in a three-dimensional array. *Nat. Phys.* **3**, 556–560 (2007).
53. Kumar, A., Wu, T.-Y., Giraldo, F. & Weiss, D. S. Sorting ultracold atoms in a 3D optical lattice in a realization of Maxwell's demon. *Nature* **561**, 83–87 (2018).
54. Browaeys, A., Barredo, D. & Lahaye, T. Experimental investigations of the dipolar interactions between a few individual Rydberg atoms. *J. Phys. B* **49**, 152001 (2016).
55. Sibalic, N., Pritchard, J. D., Adams, C. S. & Weatherill, K. J. ARC: an open-source library for calculating properties of alkali Rydberg atoms. *Comput. Phys. Commun.* **220**, 319–331 (2017).
56. Weber, S. et al. Calculation of Rydberg interaction potentials. *J. Phys. B* **50**, 133001 (2017).
57. Johnson, T. A. et al. Rabi oscillations between ground and Rydberg states with dipole–dipole atomic interactions. *Phys. Rev. Lett.* **100**, 113003 (2008).
58. Miroshnychenko, Y. et al. Coherent excitation of a single atom to a Rydberg state. *Phys. Rev. A* **82**, 013405 (2010).
59. Labuhn, H. et al. Single-atom addressing in microtraps for quantum-state engineering using Rydberg atoms. *Phys. Rev. A* **90**, 023415 (2014).
60. Jau, Y.-Y., Hankin, A. M., Keating, T., Deutsch, I. H. & Biedermann, G. W. Entangling atomic spins with a Rydberg-dressed spin-flip blockade. *Nat. Phys.* **12**, 71–74 (2016).
61. Schauss, P. et al. Observation of spatially ordered structures in a two-dimensional Rydberg gas. *Nature* **491**, 87–91 (2012).
62. Zeiher, J. et al. Microscopic characterization of scalable coherent Rydberg superatoms. *Phys. Rev. X* **5**, 031015 (2015).
63. Labuhn, H. et al. Tunable two-dimensional arrays of single Rydberg atoms for realizing quantum Ising models. *Nature* **534**, 667–670 (2016).
64. de Léséleuc, S. et al. Accurate mapping of multilevel Rydberg atoms on interacting spin-1/2 particles for the quantum simulation of Ising models. *Phys. Rev. Lett.* **120**, 113602 (2018).
65. Kim, H., Park, Y. J., Kim, K., Sim, H.-S. & Ahn, J. Detailed balance of thermalization dynamics in Rydberg-atom quantum simulators. *Phys. Rev. Lett.* **120**, 180502 (2018).
66. Lee, W., Kim, M., Jo, H., Song, Y. & Ahn, J. Coherent and dissipative dynamics of entangled few-body systems of Rydberg atoms. *Phys. Rev. A* **99**, 043404 (2019).
67. Bernien, H. et al. Probing many-body dynamics on a 51-atom quantum simulator. *Nature* **551**, 579–584 (2017).
68. Pohl, T., Demler, E. & Lukin, M. D. Dynamical crystallization in the dipole blockade of ultracold atoms. *Phys. Rev. Lett.* **104**, 043002 (2010).
69. Schauss, P. et al. Crystallization in Ising quantum magnets. *Science* **347**, 1455–1458 (2015).
70. Lienhard, V. et al. Observing the space- and time-dependent growth of correlations in dynamically tuned synthetic Ising antiferromagnets. *Phys. Rev. X* **8**, 021070 (2018).
71. Guardado-Sanchez, E. et al. Probing the quench dynamics of antiferromagnetic correlations in a 2D quantum Ising spin system. *Phys. Rev. X* **8**, 021069 (2018).
72. Keesling, A. et al. Probing quantum critical dynamics on a programmable Rydberg simulator. *Nature* **568**, 207–211 (2019).
73. Kibble, T. W. B. Topology of cosmic domains and strings. *J. Phys. A* **9**, 1387–1398 (1976).
74. Zurek, W. H. Cosmological experiments in superfluid helium? *Nature* **317**, 505–508 (1985).
75. Bouchoule, I. & Mølmer, K. Spin squeezing of atoms by the dipole interaction in virtually excited Rydberg states. *Phys. Rev. A* **65**, 041803(R) (2002).
76. Pupillo, G., Micheli, A., Boninsegni, M., Lesanovsky, I. & Zoller, P. Strongly correlated gases of Rydberg-dressed atoms: quantum and classical dynamics. *Phys. Rev. Lett.* **104**, 223002 (2010).
77. Johnson, J. E. & Rolston, S. L. Interactions between Rydberg-dressed atoms. *Phys. Rev. A* **82**, 033412 (2010).
78. Balewski, J. B. et al. Rydberg dressing: understanding of collective many-body effects and implications for experiments. *New J. Phys.* **16**, 063012 (2014).
79. Glaetzle, A. W. et al. Quantum spin-ice and dimer models with Rydberg atoms. *Phys. Rev. X* **4**, 041037 (2014).
80. Zeiher, J. et al. Coherent many-body spin dynamics in a long-range interacting Ising chain. *Phys. Rev. X* **7**, 041063 (2017).
81. Zeiher, J. et al. Many-body interferometry of a Rydberg-dressed spin lattice. *Nat. Phys.* **12**, 1095–1099 (2016).
82. Goldschmidt, E. A. et al. Anomalous broadening in driven dissipative Rydberg systems. *Phys. Rev. Lett.* **116**, 113001 (2016).
83. Boulier, T. et al. Spontaneous avalanche dephasing in large Rydberg ensembles. *Phys. Rev. A* **120**, 180502 (2018).
84. Clegg, R. M. The history of FRET. *Rev. Fluoresc.* **2006**, 1–45 (2006).
85. Giamarchi, T. *Quantum Physics in One Dimension* (Oxford Univ. Press, 2004).
86. Günter, G. et al. Observing the dynamics of dipole-mediated energy transport by interaction-enhanced imaging. *Science* **342**, 954–956 (2013).
87. Maxwell, D. et al. Storage and control of optical photons using Rydberg polaritons. *Phys. Rev. Lett.* **110**, 103001 (2013).
88. Barredo, D. et al. Coherent excitation transfer in a "spin chain" of three Rydberg atoms. *Phys. Rev. Lett.* **114**, 113002 (2015).
89. Su, W. P., Schrieffer, J. R. & Heeger, A. J. Solitons in polyacetylene. *Phys. Rev. Lett.* **42**, 1698–1701 (1979).
90. Heeger, A. J., Kivelson, S., Schrieffer, J. R. & Su, W.-P. Solitons in conducting polymers. *Rev. Mod. Phys.* **60**, 781–850 (1988).
91. Asbóth, J. K., Oroszlány, L. & Pályi, A. A short course on topological insulators: band-structure topology and edge states in one and two dimensions. Preprint at https://arxiv.org/abs/1509.02295 (2015).
92. de Léséleuc, S. et al. Observation of a symmetry-protected topological phase of interacting bosons with Rydberg atoms. *Science* **365**, 775–780 (2019).
93. Chen, X., Gu, Z.-C., Liu, Z.-X. & Wen, X.-G. Symmetry-protected topological orders in interacting bosonic systems. *Science* **338**, 1604–1606 (2012).
94. de Léséleuc, S., Barredo, D., Lienhard, V., Browaeys, A. & Lahaye, T. Analysis of imperfections in the coherent optical excitation of single atoms to Rydberg states. *Phys. Rev. A* **97**, 053803 (2018).
95. Levine, H. et al. High-fidelity control and entanglement of Rydberg atom qubits. *Phys. Rev. Lett.* **121**, 123603 (2018).
96. Brown, M. O., Thiele, T., Kiehl, C., Hsu, T.-W. & Regal, C. A. Gray-molasses optical-tweezer loading: controlling collisions for scaling atom-array assembly. *Phys. Rev. X* **9**, 011057 (2019).
97. Pagano, G. et al. Cryogenic trapped-ion system for large scale quantum simulation. *Quantum Sci. Technol.* **4**, 014004 (2019).
98. Norcia, M. A., Young, A. W. & Kaufman, A. M. Microscopic control and detection of ultracold strontium in optical-tweezer arrays. *Phys. Rev. X* **8**, 041054 (2018).
99. Cooper, A. et al. Alkaline-earth atoms in optical tweezers. *Phys. Rev. X* **8**, 041055 (2018).

100. Jackson, N. C., Hanley, R. K., Hill, M., Adams, C. S. & Jones, M. P. A. Number-resolved imaging of ^{88}Sr atoms in a long working distance optical tweezer. Preprint at https://arxiv.org/abs/1904.03233 (2019).
101. Saskin, S., Wilson, J. T., Grinkenmeyer, B. & Thomson, J. D. Narrow-line cooling and imaging of ytterbium atoms in an optical tweezer array. *Phys. Rev. Lett.* **122**, 143002 (2019).
102. Mukherjee, R., Millen, J., Nath, R., Jones, M. P. A. & Pohl, T. Many-body physics with alkaline-earth Rydberg lattices. *J. Phys. B* **44**, 184010 (2011).
103. Dunning, F. B., Killian, T. C., Yoshida, S. & Burgdörfer, J. Recent advances in Rydberg physics using alkaline-earth atoms. *J. Phys. B* **49**, 112003 (2016).
104. Nguyen, T. L. et al. Towards quantum simulation with circular Rydberg atoms. *Phys. Rev. X* **11**, 011032 (2017).
105. Lechner, W., Hauke, P. & Zoller, P. A quantum annealing architecture with all-to-all connectivity from local interactions. *Sci. Adv.* **1**, e1500838 (2015).
106. Glaetzle, A. W., van Bijnen, R. M. W., Zoller, P. & Lechner, W. A coherent quantum annealer with Rydberg atoms. *Nat. Commun.* **8**, 15813 (2017).
107. Pichler, H., Wang, S.-T., Zhou, L., Choi, S. & Lukin, M. D. Quantum optimization for maximum independent set using Rydberg atom arrays. Preprint at https://arxiv.org/abs/1808.10816 (2018).
108. Kokail, C. et al. Self-verifying variational quantum simulation of lattice models. *Nature* **569**, 355–360 (2019).
109. Preskill, J. Quantum computing in the NISQ era and beyond. *Quantum* **2**, 79–99 (2018).
110. Saffman, M. Quantum computing with atomic qubits and Rydberg interactions: progress and challenges. *J. Phys. B* **49**, 202001 (2016).
111. Weiss, D. S. & Saffman, M. Quantum computing with neutral atoms. *Phys. Today* **70**, 44–50 (2017).
112. Reinhard, A., Cubel Liebisch, T., Knuffman, B. & Raithel, G. Level shifts of rubidium Rydberg states due to binary interactions. *Phys. Rev. A* **75**, 032712 (2007).
113. Béguin, L., Vernier, A., Chicireanu, R., Lahaye, T. & Browaeys, A. Direct measurement of the van der Waals interaction between two Rydberg atoms. *Phys. Rev. Lett.* **110**, 263201 (2013).
114. Barredo, D. et al. Demonstration of a strong Rydberg blockade in three-atom systems with anisotropic interactions. *Phys. Rev. Lett.* **112**, 183002 (2014).

Acknowledgements

Competing interests

The authors declare no competing interests.

Additional information

Correspondence should be addressed to A.B.

Reprints and permissions information is available at www.nature.com/reprints.

Publisher's note Springer Nature remains neutral with regard to jurisdictional claims in published maps and institutional affiliations.